CHAPTER 37
SHAFTS

Charles R. Mischke, Ph.D., P.E.
Professor Emeritus of Mechanical Engineering
Iowa State University
Ames, Iowa

NOMENCLATURE

a	Distance
A	Area
b	Distance
c_0	Constant
C_1, C_2	Constants
d	Outside diameter of shaft
d_i	Inside diameter of hollow shaft
E	Modulus of elasticity
F	Load
g	Gravitation constant
i	index
I	Second moment of area
J	Polar second area moment
k	Torsional spring rate
K	Transverse shear stress magnification factor
K_f	Fatigue stress concentration factor
ℓ	Span

m	Mass per unit length
M	Bending moment
n	Design factor, factor of safety
p	Shrink-fit pressure
r	Load line slope
R	Bearing reaction
S_a	Strength amplitude ordinate to fatigue locus
S_e	Endurance strength
S_m	Strength steady coordinate to fatigue locus
S_y	Yield strength
S_{ut}	Ultimate tensile strength
T	Torsional or twisting moment
V	Transverse shear force
w_i	Weight of ith segment of shaft
W	Weight of shaft
x	Coordinate
x_a, x_b	Coordinates of bearings
y	Coordinate, deflection
y_0	Constant
z	Coordinate
γ	Weight density
θ	Angle
σ	Normal stress
σ'	Von Mises normal stress
τ	Shear stress
ω	First critical angular frequency

37.1 INTRODUCTION

A shaft is a rotating part used to transmit power, motion, or analogic information. It often carries rotating machine elements (gears, pulleys, cams, etc.) which assist in the transmission. A shaft is a member of a fundamental mechanical pair: the "wheel and axle." Traditional nomenclature includes

Axle A stationary member supporting rotating parts.
Shaft A rotating member supporting attached elements.
Spindle A short shaft or axle.
Head or stud shaft A shaft integral with a motor or prime mover.
Line shaft A shaft used to distribute power from one prime mover to many machines.
Jack shaft A short shaft used for power transmission as an auxiliary shaft between two other shafts (counter shaft, back shaft).

Geometric fidelity is important to many shaft functions. Distortion in a loaded body is unavoidable, and in a shaft design it is controlled so as to preserve function. There are elastic lateral displacements due to bending moment and transverse shear, and there are elastic displacements of an angular nature due to transmitted torque. Fracture due to fatigue and permanent distortion due to yielding destroy function. The tight constraint in shaft design is usually a distortion at a particular location. For example, shaft slope at a bearing centerline should typically be less than 0.001 rad for cylindrical and tapered roller bearings, 0.004 rad for deep-groove ball bearings, and 0.0087 rad for spherical ball bearings (typically). At a gear mesh, the allowable relative slope of two gears with uncrowned teeth can be held to less than 0.0005 rad each. Deflection constraints for involute gears tolerate larger (but not smaller) than theoretical center-to-center distances, with a small increase in pressure angle but with observable increases in backlash. The typical upper bound on center-to-center distance in commercial-quality spur gearing is for diametral pitches up to 10, 0.010 in; for those 11 to 19, 0.005 in; and those for 20 to 50, 0.003 in.

A harsh reality is that a deflection or slope at a shaft section is a function of the geometry and loading *everywhere*. The stress at a shaft section is a function of the local geometry and local bending moment, a simpler problem. Shaft designers often size the shaft to meet the active distortion constraint, then check for strength adequacy. Young's modulus is about the same for most shaft steels, and so adjusting the material and its condition does not significantly undo the distortional adequacy.

Shafts are proportioned so that mounted elements are assembled from one or both ends, which accounts for the stepped cylinder, fat middle aspect. This also efficiently places the most material toward the center. Shaft geometric features may also include chamfers, shoulders, grooves, keyways, splines, tapers, threads, and holes for pins and lubricant access. Shafts may even be hollow, square, etc. The effect of each of these features must be considered when checking shaft performance adequacy.

37.2 DISTORTION DUE TO BENDING

Since the most likely active constraint is a slope or a deflection at some shaft section, it is useful to determine the *constant*-diameter shaft that meets the requirement. This establishes in the designer's mind the "heft" of the shaft. Then, as one changes the local diameters and their lengths to accommodate element mounting, the material removed near the bearings has to be replaced in part, but nearer the center. It is a matter of guiding perspective at the outset. Figure 37.1 depicts shafts with a single transverse load F_i or a single point couple M_i which could be applied in either the horizontal or the vertical plane. From [37.1], Tables A-9-6 and A-9-8, expressions for slopes at each bearing can be developed. It follows by superposition that for the left bearing,

$$d = \left(\frac{32n}{3\pi E \ell \Sigma\theta} \left\{ [\Sigma F_i b_i (b_i^2 - \ell^2) + \Sigma M_i (3a_i^2 - 6a_i \ell + 2\ell^2)]_H^2 + [\Sigma F_i b_i (b_i^2 - \ell^2) + \Sigma M_i (3a_i^2 - 6a_i \ell + 2\ell^2)]_V^2 \right\}^{1/2} \right)^{1/4} \quad (37.1)$$

and for the right bearing,

$$d = \left(\frac{32n}{3\pi E \ell \Sigma\theta} \left\{ [\Sigma F_i a_i (\ell^2 - a_i^2) + \Sigma M_i (3a_i^2 - \ell^2)]_H^2 + [\Sigma F_i a_i (\ell^2 - a_i^2) + \Sigma M_i (3a_i^2 - \ell^2)]_V^2 \right\}^{1/2} \right)^{1/4} \quad (37.2)$$

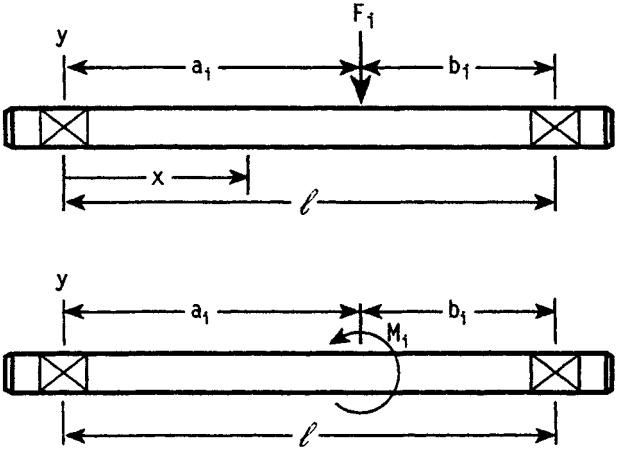

FIGURE 37.1 Simply supported shafts with force F_i and couple M_i applied.

where $\Sigma\theta$ is the absolute value of the allowable slope at the bearing. These equations are an ideal task for the computer, and once programmed interactively, are convenient to use.

Example 1. A shaft is to carry two spur gears between bearings and has loadings as depicted in Fig. 37.2. The bearing at A will be cylindrical roller. The spatial centerline slope is limited to 0.001 rad. Estimate the diameter of the uniform shaft which limits the slope at A with a design factor of 1.5.

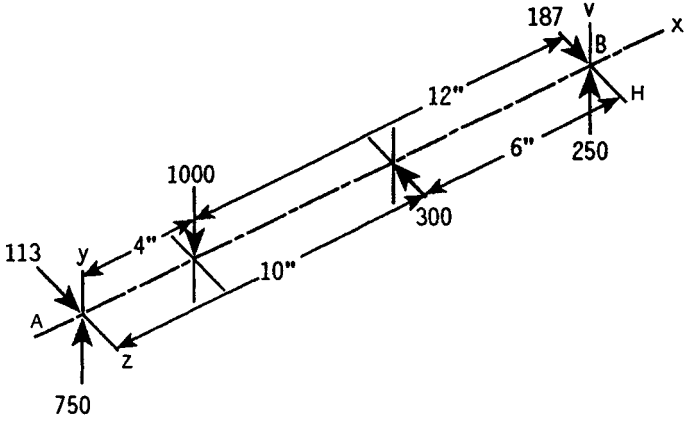

FIGURE 37.2 A shaft carries two spur gears between bearings A and B. The gear loads and reactions are shown.

Solution. Equation (37.1) is used.

$$d = \left(\frac{32n}{3\pi E \ell \Sigma \theta} \left\{ [F_1 b_1 (b_1^2 - \ell^2)]_H^2 + [F_2 b_2 (b_2^2 - \ell^2)]_V^2 \right\}^{1/2} \right)^{1/4}$$

$$= \left(\frac{32(1.5)}{3\pi 30(10)^6 \, 16(0.001)} \left\{ [300(6)(6^2 - 16^2)]^2 + [1000(12)(12^2 - 16^2)]^2 \right\}^{1/2} \right)^{1/4}$$

$$= 1.964 \text{ in}$$

Transverse bending due to forces and couples applied to a shaft produces slopes and displacements that the designer needs to control. Bending stresses account for most or all of such distortions. The effects of transverse shear forces will be addressed in Sec. 37.3.

Most bending moment diagrams for shafts are piecewise linear. By integrating once by the trapezoidal rule and a second time using Simpson's rule, one can obtain deflections and slopes that are *exact,* can be developed in tabular form, and are easily programmed for the digital computer. For bending moment diagrams that are piecewise polynomial, the degree of approximation can be made as close as desired by increasing the number of station points of interest. See [37.1], pp. 103–105, and [37.2]. The method is best understood by studying the tabular form used, as in Table 37.1.

The first column consists of station numbers, which correspond to cross sections along the shaft at which transverse deflection and slope will be evaluated. The minimum number of stations consists of those cross sections where M/EI changes in magnitude or slope, namely discontinuities in M (point couples), in E (change of material), and in I (diameter change, such as a shoulder). Optional stations include other locations of interest, including shaft ends. For integration purposes, midstation locations are chosen so that the second integration by Simpson's rule can be exact. The moment column M is dual-entry, displaying the moment as one approaches the station from the left and as one approaches from the right. The distance from the origin to a station x is single-entry. The diameter d column is dual-entry, with the entries differing at a shoulder. The modulus E column is also dual-entry. Usually the shaft is of a single material, and the column need not be filled beyond the first entry. The first integration column is single-entry and is completed by applying the trapezoidal rule to the M/EI column. The second integration column is also single-entry, using the midstation first integration data for the Simpson's rule integration.

TABLE 37.1 Form for Tabulation Method for Shaft Transverse Deflection Due to Bending Moment.

	Moment M	Dist. x	Dia. d	Modulus E	$\frac{M}{EI}$	$\int_0^x \frac{M}{EI}\,dx$	$\int_0^x \left(\int_0^x \frac{M}{EI}\,dx \right) dx$	Defl. y	Slope $\frac{dy}{dx}$
1						0	0		
2									
3									

The deflection entry y is formed from the prediction equation

$$y = \int_0^x \int_0^x \frac{M}{EI}\, dx\, dx + C_1 x + C_2 \tag{37.3}$$

The slope dy/dx column is formed from the prediction equation

$$\frac{dy}{dx} = \int_0^x \frac{M}{EI}\, dx + C_1 \tag{37.4}$$

where the constants C_1 and C_2 are found from

$$C_1 = \frac{\int_0^{x_a} \int_0^{x_a} M/(EI)\, dx\, dx - \int_0^{x_b} \int_0^{x_b} M/(EI)\, dx\, dx}{x_a - x_b} \tag{37.5}$$

$$C_2 = \frac{x_b \int_0^{x_a} \int_0^{x_a} M/(EI)\, dx\, dx - x_a \int_0^{x_b} \int_0^{x_b} M/(EI)\, dx\, dx}{x_a - x_b} \tag{37.6}$$

where x_a and x_b are bearing locations.

This procedure can be repeated for the orthogonal plane if needed, a Pythagorean combination of slope, or deflections, giving the spatial values. This is a good time to plot the end view of the deflected shaft centerline locus in order to see the spatial lay of the loaded shaft.

Given the bending moment diagram and the shaft geometry, the deflection and slope can be found at the station points. If, in examining the deflection column, any entry is too large (in absolute magnitude), find a new diameter d_{new} from

$$d_{new} = d_{old} \left| \frac{n y_{old}}{y_{all}} \right|^{1/4} \tag{37.7}$$

where y_{all} is the allowable deflection and n is the design factor. If any slope is too large in absolute magnitude, find the new diameter from

$$d_{new} = d_{old} \left| \frac{n(dy/dx)_{old}}{(\text{slope})_{all}} \right|^{1/4} \tag{37.8}$$

where $(\text{slope})_{all}$ is the allowable slope. As a result of these calculations, find the largest d_{new}/d_{old} ratio and multiply all diameters by this ratio. The tight constraint will be at its limit, and all others will be loose. Don't be concerned about end journal size, as its influence on deflection is negligible.

Example 2. A shaft with two loads of 600 and 1000 lbf in the same plane 2 inches (in) inboard of the bearings and 16 in apart is depicted in Fig. 37.3. The loads are from 8-pitch spur gears, and the bearings are cylindrical roller. Establish a geometry of a shaft which will meet distortion constraints, using a design factor of 1.5.

Solution. The designer begins with identification of a uniform-diameter shaft which will meet the likely constraints of bearing slope. Using Eq. (37.2), expecting the right bearing slope to be controlling,

$$d = \left[\frac{32(1.5)}{3\pi 30(10)^6 16(0.001)} \left| 600(2)(16^2 - 2^2) + 1000(14)(16^2 - 14^2) \right| \right]^{1/4}$$

$$= 1.866 \text{ in}$$

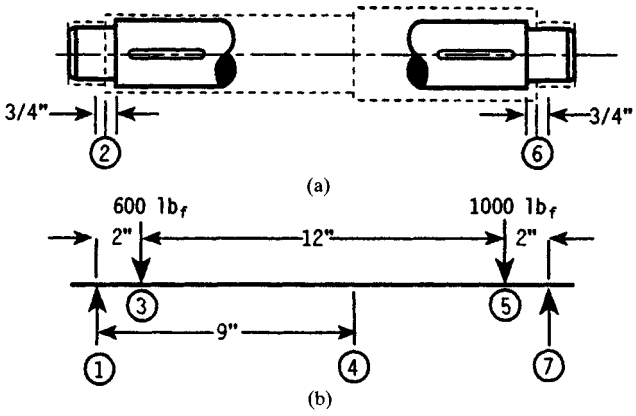

FIGURE 37.3 (*a*) The solid-line shaft detail is the designer's tentative geometry. The dashed lines show shaft sized to meet bending distortion constraints. (*b*) The loading diagram and station numbers.

Based on this, the designer sketches in some tentative shaft geometry as shown in Fig. 37.3*a*. The designer decides to estimate the bearing journal size as 1.5 in, the next diameter as 1.7 in, the diameter beyond a shoulder 9 in from the left bearing as 1.9 in, and the remaining journal as 1.5 in. The next move is to establish the moment diagram and use seven stations to carry out the tabular deflection method by completing Table 37.1. Partial results are shown below.

Station	x, in	Moment M, in · lbf	Diameter d, in	Deflection y, in	Slope dy/dx
1	0	0	1.5	0	–0.787E-03
2	0.75	487.5	1.5/1.7	–0.584E-03	–0.763E-03
3	2	1300	1.7	–0.149E-02	–0.672E-03
4	9	1650	1.7/1.9	–0.337E-02	0.168E-03
5	14	1900	1.9	–0.140E-02	0.630E-03
6	15.25	712.5	1.9/1.5	–0.554E-03	0.715E-03
7	16	0	1.5	0	0.751E-03

The gears are 8 pitch, allowing 0.010/2 = 0.005 in growth in center-to-center distance, and both y_3 and y_5 have absolute values less than 0.005/1.5 = 0.00333, so that constraint is loose. The slope constraints of 0.001/1.5 are violated at stations 1 and 7, so using Eq. (37.8),

$$(d_1)_{\text{new}} = 1.5\left|\frac{1.5(-0.000\,787)}{0.001}\right|^{1/4} = 1.5(1.042)\text{ in}$$

$$(d_7)_{\text{new}} = 1.5\left|\frac{1.5(0.000\,751)}{0.001}\right|^{1/4} = 1.5(1.030)\text{ in}$$

and the gear mesh slope constraints are violated at stations 3 and 5, so using Eq. (37.8),

$$(d_3)_{\text{new}} = 1.7\left|\frac{1.5(0.001\,49)}{0.0005}\right|^{1/4} = 1.7(1.454)\text{ in}$$

$$(d_5)_{\text{new}} = 1.9\left|\frac{1.5(0.001\,40)}{0.0005}\right|^{1/4} = 1.9(1.432)\text{ in}$$

The largest d_{new}/d_{old} ratio among the four violated constraints is 1.454, so *all* diameters are multiplied by 1.454, making $d_1 = 1.5(1.454) = 2.181$ in, $d_3 = 1.7(1.454) = 2.472$ in, $d_5 = 1.9(1.454) = 2.763$ in, and $d_7 = 1.5(1.454) = 2.181$ in. The diameters d_1 and d_7 can be left at 1.5 or adjusted to a bearing size without tangible influence on transverse deflection or slope. One also notes that the largest multiplier 1.454 is associated with the now tight constraint at station 3, all others being loose. Rounding d_3 and/or d_5 up will render all bending distortion constraints loose.

37.3 DISTORTION DUE TO TRANSVERSE SHEAR

Transverse deflection due to transverse shear forces associated with bending becomes important when the the shaft length-to-diameter ratio is less than 10. It is a short-shaft consideration. A method for estimating the shear deflection is presented in Ref. [37.2]. There are two concerns associated with shear deflection. The first is that it is often forgotten on short shafts. The second is that it is often neglected in formal education, and engineers tend to be uncomfortable with it. Ironically, it is simpler than bending stress deflection.

The loading influence is the familiar shear diagram. The transverse shear force V is piecewise linear, and the single integration required is performed in a tabular method suitable to computer implementation. Table 37.2 shows the form. The left-hand column consists of station numbers which identify cross sections along the shaft at which shear deflection and slope are to be estimated. The minimum number of stations consists of those cross sections where $KV/(AG)$ changes abruptly, namely at discontinuities in transverse shear force V (at loads), in cross-sectional area A (at shoulders), and in torsional modulus G (if the material changes). Optional stations include other locations of interest. There is no need for midstation locations, since the trapezoidal rule will be used for integration, maintaining exactness. The shear force column V is dual-entry, the location x is single-entry, and the diameter d column is dual-entry, as is the torsional modulus G column, if included. The $KV/(AG)$ column is dual-entry, as is the slope dy/dx column.

The single-entry integral column is generated using the trapezoidal rule. The single-entry deflection column y is generated from the prediction equation

$$y = \int_0^x \frac{KV}{AG}\,dx + c_0 x + y_0 \tag{37.9}$$

TABLE 37.2 Form for Tabulation Method for Shaft Transverse Deflection Due to Transverse Shear.

	Shear V	Dist. x	Dia. d	Modulus G	$\frac{KV}{AG}$	$\int_0^x \frac{KV}{AG}\,dx$	Defl. y	Slope $\frac{dy}{dx}$	Avg. slope $(dy/dx)_{av.}$
1						0			
2									
3									
4									

The dual-entry slope dy/dx column is generated from the other prediction equation,

$$\frac{dy}{dx} = -\frac{KV}{AG} + c_0 \tag{37.10}$$

where

$$c_0 = \frac{\int_0^{x_a} KV/(AG)\,dx - \int_0^{x_b} KV/(AG)\,dx}{x_a - x_b} \tag{37.11}$$

$$y_0 = \frac{x_a \int_0^{x_b} KV/(AG)\,dx - x_b \int_0^{x_a} KV/(AG)\,dx}{x_a - x_b} \tag{37.12}$$

where x_a and x_b are bearing locations and K is the factor 4/3 for a circular cross section (the peak stress at the centerline is 4/3 the average shear stress on the section). The slope column can have dual entries because Eq. (37.10) contains the discontinuous $KV/(AG)$ term.

Example 3. A uniform 1-in-diameter stainless steel [$G = 10(10)^6$ psi] shaft is loaded as shown in Fig. 37.4 by a 1000-lbf overhung load. Estimate the shear deflection and slope of the shaft centerline at the station locations.

Solution. Omitting the G column, construct Table 37.3. After the integral column is complete, c_0 and y_0 are given by Eqs. (37.11) and (37.12), respectively:

$$c_0 = \frac{0 - 339.5(10^{-6})}{1 - 11} = 33.95(10^{-6})$$

$$y_0 = \frac{1(339.5)10^{-6} - 11(0)}{1 - 11} = -33.95(10^{-6})$$

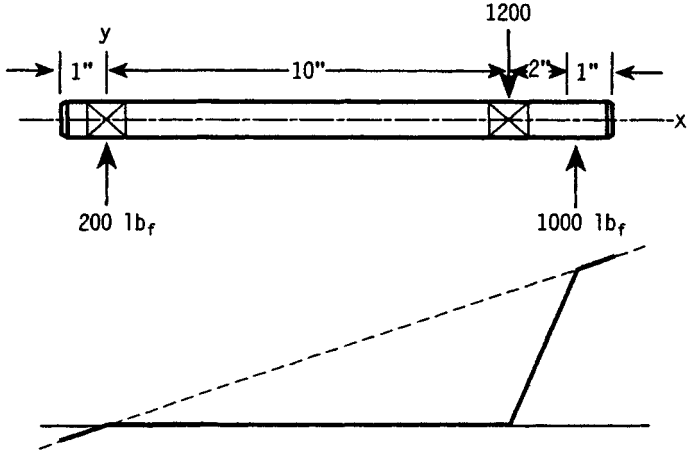

FIGURE 37.4 A short uniform shaft, its loading, and shear deflection.

TABLE 37.3 Transverse Shear Deflection in Shaft of Fig. 37.4

Station	V	x	d	$\frac{KV}{AG}$	$\int_0^x \frac{KV}{AG}\,dx$	y	dy/dx	$(dy/dx)_{av}$
1	0	0	0	0	0	–33.95E-06	33.95E-06	33.95E-06
	0		1	0			33.95E-06	
2	0	1	1	0	0	0	33.95E-06	16.98E-06
	200		1	33.95E-06			0	
3	200	11	1	33.95E-06	339.5E-06	0	0	101.9E-06
	–1000		1	–169.8E-06			203.75E-06	
4	–1000	13	1	–169.8E-06	0	407.4E-06	203.75E-06	118.9E-06
	0		1	0			33.95E-06	
5	0	14	1	0	0	441.4E-06	33.95E-06	33.95E-06
	0		0	0			33.95E-06	

The prediction Eqs. (37.9) and (37.10) are

$$y = -\int_0^x \frac{KV}{AG}\,dx + 33.95(10^{-6})x - 33.95(10^{-6})$$

$$\frac{dy}{dx} = 33.95(10^{-6}) - \frac{KV}{AG}$$

and the rest of the table is completed.

A plot of the shear deflection curve is shown under the shaft in Fig. 37.4. Note that it is piecewise linear. The droop of the unloaded overhang is a surprise when the between-the-bearings shaft is straight and undeflected. The discontinuous curve arises from discontinuities in loading V. In reality, V is not discontinuous, but varies rapidly with rounded corners. If a rolling contact bearing is mounted at station 2, the bearing inner race will adopt a compromise angularity between $dy/dx = 33.95(10^{-6})$ and $dy/dx = 0$. This is where the average (midrange) slope $(dy/dx)_{av}$ is useful in estimating the extant slope of the inner race with respect to the outer race of the bearing.

Figure 37.5 shows a short shaft loading in bending. Table 37.4 shows the deflection analysis of Sec. 37.2 for this shaft in columns 3 and 4, the shear deflection analysis of Sec. 37.3 in columns 5 and 6, and their superposition in columns 7 and 8. Figure 37.5 shows the shear deflection at station 7 to be about 28 percent of the bending deflection, and the shear slope at station 9 to be about 15 percent of the bending slope. Both of these locations could involve an active constraint. In the deflection analysis of shafts with length-to-diameter aspect ratios of less than 10, the transverse shear deflections should be included.

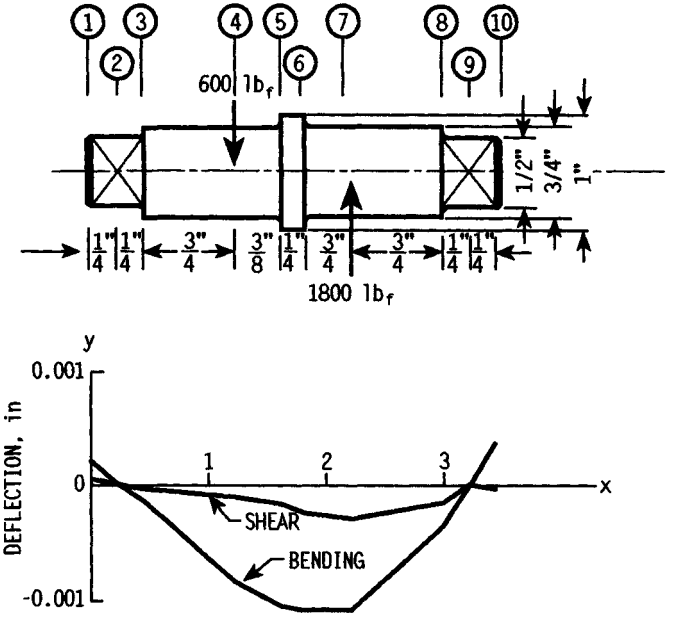

FIGURE 37.5 A short shaft of several diameters, its loading, and the consequential shear and bending deflections.

TABLE 37.4 Deflections of Shaft of Fig. 37.5

Station	x_i	Bending† y_i	Bending $(dy/dx)_i$	Shear‡ y_i	Shear $(dy/dx)_{avi}$	Combined y_i	Combined $(dy/dx)_i$
1		0.000 240	–0.000 959	0.738E-05	–0.295E-04	0.247E-03	–0.988E-03
2	0.250	0	–0.000 959	0	–0.886E-04	0	–0.105E-02
3	0.500	–0.000 234	–0.000 891	–0.369E-04	–0.115E-03	–0.271E-03	–0.101E-02
4	1.250	–0.000 842	–0.000 690	–0.984E-04	–0.116E-03	–0.940E-03	–0.850E-03
5	1.625	–0.001 05	–0.000 408	–0.188E-03	–0.194E-03	–0.124E-02	–0.601E-03
6	1.875	–0.001 14	–0.000 306	–0.225E-03	–0.194E-03	–0.137E-02	–0.500E-03
7	2.250	–0.001 14	0.000 378	–0.315E-03	–0.328E-05	–0.145E-02	0.375E-03
8	3.000	–0.000 403	0.001 38	–0.140E-03	0.397E-03	–0.543E-03	0.178E-02
9	3.250	0	0.001 72	0	0.266E-03	0	0.199E-02
10	3.500	0.000 431	0.001 72	–0.738E-05	–0.295E-04	0.424E-03	0.169E-02

† $C_1 = -0.959(10^{-3})$, $C_2 = 0.240(10^{-3})$, Eqs. (37.5) and (37.6).
‡ $c_0 = -0.295(10^{-4})$, $y_0 = 0.738(10^{-5})$, Eqs. (37.11) and (37.12).

37.4 DISTORTION DUE TO TORSION

Angular deflection in a right circular cylindrical shaft due to torque T is

$$\theta = \frac{T\ell}{GJ} \quad \text{rad} \tag{37.13}$$

For a stepped shaft of individual cylinder length ℓ_i with torques T_i, the angular deflection is

$$\theta = \Sigma\theta_i = \Sigma \frac{T_i \ell_i}{G_i J_i} \tag{37.14}$$

which becomes $\theta = (T/G)\Sigma(\ell_i/J_i)$ for constant torque through homogeneous material. The torsional stiffness can be defined as $k_i = T_i/\theta_i$, and since $\theta_i = T_i/k_i$ and $\theta = \Sigma\theta_i = \Sigma(T_i/k_i)$, one may write for constant torque $\theta = T\Sigma(1/k_i)$. It follows that

$$\frac{1}{k} = \Sigma \frac{1}{k_i} \tag{37.15}$$

The equation $\theta = (T/G)\Sigma\ell_i/J_i$ is not precise, since experimental evidence shows that θ is larger than given by this equation.

The material in a step (shoulder) has a surface free of shear. Some material loafs, so other material is more distressed and distorts more. The existence of keyways, splines, and tapered sections increases angular flexibility also. For quantitative treatment of these realities, see Ref. [37.3], pp. 93–99. When a coupling is keyed or splined to a shaft, that shaft can be considered to twist independently of the coupling for one-third of its hub length.

37.5 SHAFT MATERIALS

Most steels have similar moduli of elasticity, so that the rigidity requirement can be met by geometric decisions, independent of the material choice among steels. Strength to resist loading stresses affects the choice of material. ANSI 1020-1050 steels and 11XX free-machining steels are common choices. Heat treating 1340-50, 3140-50, 4140, 4340, 5140, and 8650 steels produces greater strength. Hardness is a function of size, and the methods of Grossman and Fields and of Crafts and Lamont in Chapter 8 are important to quantitatively relate strength to size and heat-treatment regimen. Carburizing grades 1020, 4320, 4820, and 8620 are chosen for surface-hardening purposes.

Cold-rolled sections are available up to about 3½ in in diameter. Hot-rolled rounds are available up to nearly 6 in. Above this size, forging precedes machining.

When a shaft geometry is created (prior to final machining) by a volume-conservative process (casting or hot or cold forming), then optimality can be pursued by minimizing the material amount if production volume permits. Constraints can be made nearly active at several locations. Many shafts are created for small production runs by machining round stock, and optimality may be achieved by minimizing the amount of material removed from the work piece, which minimizes the machining effort.

37.6 LOAD-INDUCED STRESSES

Shafts that transmit power are often loaded in such a way that the torsion which performs the work induces transverse bending forces at gears. If the torsion is stochastic, so is the induced bending due to pitch-line forces. Both the torsion and the bending moment have the same distribution and coefficient of variation. The same is true of a point couple induced at a helical gear.

For ductile shaft materials, distortion energy theory is used, and the array of stresses at a critical location element are combined to form the von Mises stress. If the normal stresses at a point are σ_x, σ_y, σ_z and the associated shear stresses are τ_{xy}, τ_{yz}, τ_{zx}, then the von Mises stress σ' is given by

$$\sigma' = \frac{1}{\sqrt{2}}[(\sigma_x - \sigma_y)^2 + (\sigma_y - \sigma_z)^2 + (\sigma_z - \sigma_x)^2 + 6(\tau_{xy}^2 + \tau_{yz}^2 + \tau_{zx}^2)]^{1/2} \quad (37.16)$$

In a shaft, the critical location is usually at a surface, and two normal stresses (say σ_y and σ_z) and two shear stresses (say τ_{xz} and τ_{zx}) are zero. Equation (37.16) simplifies to

$$\sigma' = (\sigma_x^2 + 3\tau_{xy}^2)^{1/2} \quad (37.17)$$

The bending stress σ_x is usually expressed as $32K_fM/(\pi d^3)$ and the shear stress τ_{xy} is expressed as $16K_f'T/(\pi d^3)$, or without the stress concentration K_f' if torsion is steady, and so Eq. (37.17) is written as

$$\sigma' = \left[\left(\frac{32K_fM}{d^3}\right)^2 + 3\left(\frac{16T}{d^3}\right)^2\right]^{1/2} \quad (37.18)$$

As the shaft rotates and the stress field remains stationary, the bending moment induces a completely reversed stress σ_x on the rotating element in Fig. 37.6. The amplitude component of this stress σ_a' is

$$\sigma_a' = \left|\frac{32K_fM_a}{\pi d^3}\right| \quad (37.19)$$

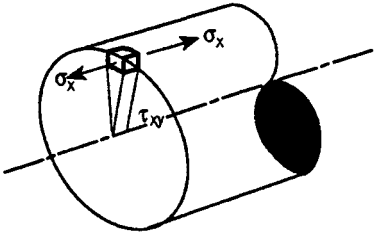

FIGURE 37.6 A stress element at a shaft surface.

The subscript on M_a is to designate the bending moment inducing a completely reversed normal stress on the element as the shaft turns. The bending moment itself may indeed be steady. The steady component of stress σ_m', from Eq. (37.18), is

$$\sigma_m' = \left|\frac{16\sqrt{3}\,T_m}{\pi d^3}\right| \quad (37.20)$$

The stochastic nature of $\mathbf{K}_f$, $\mathbf{M}_a$, and $\mathbf{d}$ controls the nature of $\boldsymbol{\sigma}_a'$. Usually the geometric variation in $\mathbf{d}$ involves coefficients of variation of 0.001 or less, and that of $\mathbf{K}_f$ and $\mathbf{M}_a$ is more than an order of magnitude higher, and so $\mathbf{d}$ is usually considered deterministic. The distribution of $\boldsymbol{\sigma}_a'$ depends on the distributions of $\mathbf{K}_f$ and $\mathbf{M}_a$. When $\mathbf{M}_a$ is lognormal (and since $\mathbf{K}_f$ is robustly lognormal), the distribution of $\boldsymbol{\sigma}_a'$ is lognormal. When $\mathbf{M}_a$ is not lognormal, then a computer simulation will give the stochastic information on $\boldsymbol{\sigma}_a'$.

A press fit induces a surface pressure p and a hoop normal stress of $-p$, so the three orthogonal normal stresses are σ_x, $-p$, and $-p$, and Eq. (37.16) becomes

$$\sigma' = \frac{1}{\sqrt{2}}\{[\sigma_x - (-p)]^2 + [-p - (-p)]^2 + (-p - \sigma_x)^2 + 6\tau_{xy}^2\}^{1/2}$$

$$\sigma' = [(\sigma_x + p)^2 + 3\tau_{xy}^2]^{1/2}$$

The amplitude and steady components of the von Mises stress at a surface element in a press fit are, respectively,

$$\sigma'_a = (\sigma_x^2)^{1/2} = \sigma_x \tag{37.21}$$

$$\sigma'_m = (p^2 + 3\,\tau_{xy}^2)^{1/2} \tag{37.22}$$

On the designer's fatigue diagram, the σ'_a, σ'_m coordinates don't necessarily define a point because certain geometric decisions may not yet have been made. In such cases, a locus of possible points which is called the *load line* is established. Often the load line includes the origin, and so the slope together with one point on the line defines the load line. Its slope r is the ratio σ'_a/σ'_m.

37.7 STRENGTH

For the first-quadrant fatigue locus on the designer's fatigue diagram, effective regression models include the 1874 Gerber parabola and the recent ASME-elliptic locus, both of which lie in and among the data. The Gerber parabola is written as

$$\frac{n\sigma_a}{S_e} + \left(\frac{n\sigma_m}{S_{ut}}\right)^2 = 1 \tag{37.23}$$

and the failure locus itself, substituting $n\sigma_a = S_a$ and $n\sigma_m = S_m$ in Eq. (37.23), is expressible as

$$\frac{S_a}{S_e} + \left(\frac{S_m}{S_{ut}}\right)^2 = 1 \tag{37.24}$$

Combining the damaging stress [distortion energy von Mises stress, Eqs. (37.19) and (37.20)] with the strengths in Eq. (37.23) leads to

$$d = \left\{\frac{16nK_fM_a}{\pi S_e}\left[1 + \sqrt{1 + 3\left(\frac{T_mS_e}{K_fM_aS_{ut}}\right)^2}\right]\right\}^{1/3} \tag{37.25}$$

$$\frac{1}{n} = \frac{16K_fM_a}{\pi d^3 S_e}\left[1 + \sqrt{1 + 3\left(\frac{T_mS_e}{K_fM_aS_{ut}}\right)^2}\right] \tag{37.26}$$

Equations (37.25) and (37.26) are called distortion energy–Gerber equations, or D.E.–Gerber equations.

The ASME-elliptic of Ref. [37.4] has a fatigue locus in the first quadrant expressed as

$$\left(\frac{n\sigma_a}{S_e}\right)^2 + \left(\frac{n\sigma_m}{S_y}\right)^2 = 1 \tag{37.27}$$

and the fatigue locus itself is expressed as

$$\left(\frac{S_a}{S_e}\right)^2 + \left(\frac{S_m}{S_y}\right)^2 = 1 \tag{37.28}$$

Combining Eqs. (37.19) and (37.20) with (37.28) gives

$$d = \left\{\frac{32n}{\pi}\left[\left(\frac{K_f M_a}{S_e}\right)^2 + \frac{3}{4}\left(\frac{T_m}{S_y}\right)^2\right]^{1/2}\right\}^{1/3} \tag{37.29}$$

$$\frac{1}{n} = \frac{32}{\pi d^3}\left[\left(\frac{K_f M_a}{S_e}\right)^2 + \frac{3}{4}\left(\frac{T_m}{S_y}\right)^2\right]^{1/2} \tag{37.30}$$

which are called D.E.–elliptic or ASME-elliptic equations.

On the designer's fatigue diagram, the slope of a radial load line r is given by

$$r = \frac{\sigma_a'}{\sigma_m'} = \frac{32K_f M_a}{\pi d^3} \cdot \frac{\pi d^3}{16\sqrt{3}T_m} = \frac{2}{\sqrt{3}}\frac{K_f M_a}{T_m} \tag{37.31}$$

The expressions for d and n in Eqs. (37.29) and (37.30) are for a threat from fatigue failure. It is also possible on the first revolution to cause local yielding, which changes straightness and strength and involves now-unpredictable loading. The Langer line, $S_a + S_m = S_y$, predicts yielding on the first cycle. The point where the elliptic locus and the Langer line intersect is described by

$$\frac{S_a}{S_e} = \frac{2S_e/S_y}{1 + (S_e/S_y)^2} \tag{37.32}$$

$$\frac{S_m}{S_y} = \frac{1 - (S_e/S_y)^2}{1 + (S_e/S_y)^2} \tag{37.33}$$

The *critical slope* contains this point:

$$r_{\text{crit}} = \frac{2(S_e/S_y)^2}{1 - (S_e/S_y)^2} \tag{37.34}$$

If the load line slope r is greater than r_{crit}, then the threat is from fatigue. If r is less than r_{crit}, the threat is from yielding.

For the Gerber fatigue locus, the intersection with the Langer line is described by

$$S_a = \frac{S_{ut}^2 - 2S_e S_y}{2S_e}\left[-1 + \sqrt{1 + \frac{4(S_{ut}^2 - S_y^2)}{(S_{ut}^2/S_e - 2S_y)^2}}\right] \tag{37.35}$$

$$S_m = \frac{S_{ut}^2}{2S_e}\left[1 - \sqrt{1 + \frac{4S_e^2(1 - S_y/S_e)}{S_{ut}^2}}\right] \tag{37.36}$$

and $r_{\text{crit}} = S_a/S_m$.

Example 4. At the critical location on a shaft, the bending moment M_a is 2520 in · lbf and the torque T_m is 6600 in · lbf. The ultimate strength S_{ut} is 80 kpsi, the yield strength S_y is 58 kpsi, and the endurance limit S_e is 31.1 kpsi. The stress concentration

factor corrected for notch sensitivity K_f is 1.54. Using an ASME-elliptic fatigue locus, ascertain if the threat is from fatigue or yielding.

Solution. From Eq. (37.31),

$$r = \frac{2(1.54)2520}{\sqrt{3}\,6600} = 0.679$$

From Eq. (37.34),

$$r_{\text{crit}} = \frac{2(31.1/58)^2}{1-(31.1/58)^2} = 0.807$$

Since $r_{\text{crit}} > r$, the primary threat is from fatigue. Using the Gerber fatigue locus, $r_{\text{crit}} = S_a/S_m = 26.18/31.8 = 0.823$.

For the distortion energy–Gerber failure locus, the relation for the strength amplitude S_a is given in Eq. (13.34) and C_{Sa} in Eq. (13.35); these quantities are given by Eqs. (13.37) and (13.38), respectively, for the ASME-elliptic failure locus.

37.8 CRITICAL SPEEDS

Critical speeds are associated with uncontrolled large deflections, which occur when inertial loading on a slightly deflected shaft exceeds the restorative ability of the shaft to resist. Shafts must operate well away from such speeds. Rayleigh's equation for the first critical speed of a shaft with transverse inertial loads w_i deflected y_i from the axis of rotation for simple support is given by Ref. [37.6] as

$$\omega = \sqrt{\frac{g\Sigma w_i y_i}{\Sigma w_i y_i^2}} \tag{37.37}$$

where w_i is the inertial load and y_i is the lateral deflection due to w_i and *all other loads.* For the shaft itself, w_i is the inertial load of a shaft section and y_i is the deflection of the center of the shaft section due to all loads. Inclusion of shaft mass when using Eq. (37.37) can be done.

Reference [37.7], p. 266, gives the first critical speed of a uniform simply supported shaft as

$$\omega = \frac{\pi^2}{\ell^2}\sqrt{\frac{EI}{m}} = \frac{\pi^2}{\ell^2}\sqrt{\frac{gEI}{A\gamma}} \tag{37.38}$$

Example 5. A steel thick-walled tube with 3-in OD and 2-in ID is used as a shaft, simply supported, with a 48-in span. Estimate the first critical speed (*a*) by Eq. (37.38) and (*b*) by Eq. (37.37).

Solution. (*a*) $A = \pi(3^2 - 2^2)/4 = 3.927$ in^2, $I = \pi(3^4 - 2^4)/64 = 3.19$ in^4, $w = A\gamma = 3.925(0.282) = 1.11$ lbf/in. From Eq. (37.38),

$$\omega = \frac{\pi^2}{48^2}\sqrt{\frac{386(30)(10^6)(3.19)}{3.927(0.282)}} = 782.4 \text{ rad/s} = 7471 \text{ r/min}$$

(*b*) Divide the shaft into six segments, each 8 in long, and from the equation for the deflection at x of a uniformly loaded, simply supported beam, develop an expression for the deflection at x.

$$y = \frac{wx}{24EI}(2\ell x^2 - x^3 - \ell^3) = \frac{1.11x}{24(30)(10^6)(3.19)}[2(48)x^2 - x^3 - 48^3]$$

$$= 0.483(10^{-9})(x)(96x^2 - x^3 - 48^3)$$

Prepare a table for x, y, and y^2 at the six stations.

x_i	y_i	y_i^2
4	0.000 210 8	$4.44(10^{-8})$
12	0.000 570 9	$32.6(10^{-8})$
20	0.000 774 7	$60.0(10^{-8})$
28	0.000 774 7	$60.0(10^{-8})$
36	0.000 570 9	$32.6(10^{-8})$
44	0.000 210 8	$4.44(10^{-8})$
Σ	0.003 112 8	$194(10^{-8})$

From Eq. (37.37),

$$\omega = \sqrt{\frac{g\Sigma y_i}{\Sigma y_i^2}} = \sqrt{\frac{386(0.003\,112\,8)}{194(10^{-8})}} = 787 \text{ rad/s} = 7515 \text{ r/min}$$

which agrees with the result of part (*a*), but is slightly higher, as expected, since the static deflection shape was used.

Since most shafts are of variable diameter, Eq. (37.37) will be more useful for estimating the first critical speed, treating simultaneously the contributions of concentrated masses (gears, pulleys, sprokets, cams, etc.) and the distributed shaft mass as well.

Example 6. Assume that the shaft of Example 2 has been established with its final geometry as shown in Fig. 37.7. The shaft is decomposed into 2-in segments. The weight of each segment is applied as a concentrated force w_i at the segment centroid. Additionally, the left-side gear weighs 30 lbf and the right-side gear weighs 40 lbf. Estimate the first critical speed of the assembly.

Solution. Bearing in mind the tabular deflection method of Sec. 37.2, twelve stations are established. Also, bending moment diagrams will be superposed.

For the distributed shaft mass load, the shaft weight is estimated as $W = 24.52$ lbf, and it follows that bearing reactions are $R_1' = 11.75$ lbf and $R_2' = 12.77$ lbf. Because each reaction is opposed by a bearing seat weight of 1.772 lbf, the net reactions are $R_1 = 11.75 - 1.722 = 9.98$ lbf and $R_2 = 12.77 - 1.772 = 11.0$ lbf. The bending moments M_i due to shaft segment weights are shown in column 3 of Table 37.5.

For the gears, $R_1 = 31.25$ lbf and $R_2 = 38.75$ lbf, and the resulting bending moments are shown in column 4. The superposition of the moment diagrams for these two sources of bending occurs in column 5. Column 6 displays the shaft segment weights at the station of application. Column 7 shows the concentrated gear weights and their station of application. Column 8 is the superposition of columns 6 and 7. Column 9 is obtained by using the tabular method of Sec. 37.2 and imposing the bending moment diagram of column 5. Columns 10 and 11 are extensions of columns 8 and 9. The sums of columns 10 and 11 are used in Eq. (37.37):

$$\omega = \sqrt{\frac{386(2.348)(10^{-3})}{6.91(10^{-8})}} = 3622 \text{ rad/s} = 34\,588 \text{ r/min}$$

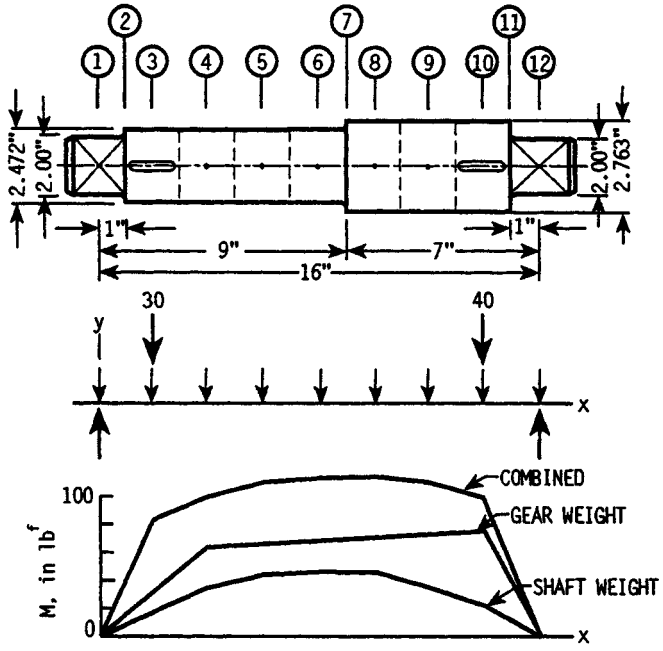

FIGURE 37.7 The final geometry of the shaft of Ex. 37.2. For critical speed estimation, weights of shaft segments and affixed gears generate separate and combined bending moments. The static deflection under such loading found by the tabulation method provides the deflections used in Rayleigh's critical speed equation. See Table 37.5 and Ex. 37.6.

The methods of Secs. 37.2 and 37.3 and this section can be programmed for the digital computer for rapid and convenient use.

37.9 HOLLOW SHAFTS

Advantages accruing to hollow shafting include weight reduction with minor increase in stress (for the same outside diameter), ability to circulate fluids for lubrication or cooling, and the use of thick-walled tubing as shaft stock. However, unbalance must be checked and corrected, and thick-walled tubing may not have enough material in its wall to accommodate the desired external geometry.

For a shaft section with outside diameter d, inside diameter d_i, and $K = d_i/d$, for torsional and bending loading, $d(1 - K^4)^{1/3}$ may be substituted for diameter d in equations such as (37.25), (37.26), (37.29), and (37.30). Equations (37.25) and (37.29) can no longer be solved explicitly for diameter d unless K is known. In cases where it is not known, iterative procedures must be used.

TABLE 37.5 Critical Speed Tabulation for Example 7

Station	x_i	Distributed load M_i	Gear M_i	Super-posed M_i	Shaft section w_i	Concentrated load P_i	Super -posed w_i	Tabulation† method y_i	$w_i y_i$	$w_i y_i^2$
1	0	0	0	0	1.772		1.772	0	0	0
2	1	9.98	31.25	41.23				−0.122E-04		
3	2	19.96	62.5	82.46	2.707	30	32.07	−0.233E-04	0.747E-03	1.741E-08
4	4	34.51	65.0	99.51	2.707		2.707	−0.411E-04	0.111E-03	0.457E-08
5	6	43.64	67.5	111.14	2.707		2.707	−0.517E-04	0.140E-03	0.724E-08
6	8	47.36	70.0	117.36	2.707		2.707	−0.543E-04	0.147E-03	0.798E-08
7	9	46.51	71.25	117.76				−0.524E-04		
8	10	45.66	72.5	118.16	3.382		3.382	−0.488E-04	0.165E-03	0.805E-08
9	12	37.20	75.0	112.2	3.382		3.382	−0.375E-04	0.127E-03	0.476E-08
10	14	21.98	77.5	99.48	3.382	40	43.382	−0.210E-04	0.911E-03	1.913E-08
11	15	10.99	38.75	49.74				−0.110E-04		
12	16	0	0	0	1.772		1.772	0	0	0
									2.348E-03	6.91E-08

† Column 9 obtained by tabular method of Sec. 37.2. The constants $C_1 = -0.1249\text{E-}04$ and $C_2 = 0$ of prediction Eqs. (37.5) and (37.6) were used.

REFERENCES

37.1 Joseph E. Shigley and Charles R. Mischke, *Mechanical Engineering Design,* 5th ed., McGraw-Hill, New York, 1989.

37.2 Charles R. Mischke, "An Exact Numerical Method for Determining the Bending Deflection and Slope of Stepped Shafts," *Advances in Reliability and Stress Analysis,* Proceedings of the Winter Annual Meeting of A.S.M.E., San Francisco, December 1978, pp. 105–115.

37.3 R. Bruce Hopkins, *Design Analysis of Shafts and Beams,* McGraw-Hill, New York, 1970, pp. 93–99.

37.4 ANSI/ASME B106.1-M-1985, "Design of Transmission Shafting," second printing, March 1986.

37.5 S. Timoshenko, D. H. Young, and W. Weaver, *Vibration Problems in Engineering,* 4th ed., John Wiley & Sons, New York, 1974.

37.6 S. Timoshenko and D. H. Young, *Advanced Dynamics,* McGraw-Hill, New York, 1948, p. 296.

37.7 Charles R. Mischke, *Elements of Mechanical Analysis,* Addison-Wesley, Reading, Mass., 1963.

RECOMMENDED READING

ANSI B17.1, 1967, "Keys and Keyseats."

Mischke, Charles R., "A Probabilistic Model of Size Effect in Fatigue Strength of Rounds in Bending and Torsion," *Transactions of A.S.M.E., Journal of Mechanical Design,* vol. 102, no. 1, January 1980, pp. 32–37.

Peterson, R. E., *Stress Concentration Factors,* John Wiley & Sons, New York, 1974.

Pollard, E. I., "Synchronous Motors . . . , Avoid Torsional Vibration Problems," *Hydrocarbons Processing,* February 1980, pp. 97–102.

Umasankar, G., and C. R. Mischke, "A Simple Numerical Method for Determining the Sensitivity of Bending Deflections of Stepped Shafts to Dimensional Changes," *Transactions of A.S.M.E., Journal of Vibration, Acoustics, Stress and Reliability in Design,* vol. 107, no. 1, January 1985, pp. 141–146.

Umasankar, G., and C. Mischke, "Computer-Aided Design of Power Transmission Shafts Subjected to Size, Strength and Deflection Constraints Using a Nonlinear Programming Technique," *Transactions of A.S.M.E., Journal of Vibration, Acoustics, Stress and Reliability in Design,* vol. 107, no. 1, January 1985, pp. 133–140.